

The fate of scattered planets

Benjamin C. Bromley

*Department of Physics & Astronomy, University of Utah,
115 S 1400 E, Rm 201, Salt Lake City, UT 84112*

bromley@physics.utah.edu

Scott J. Kenyon

*Smithsonian Astrophysical Observatory,
60 Garden St., Cambridge, MA 02138*

skenyon@cfa.harvard.edu

ABSTRACT

As gas giant planets evolve, they may scatter other planets far from their original orbits to produce hot Jupiters or rogue planets that are not gravitationally bound to any star. Here, we consider planets cast out to large orbital distances on eccentric, bound orbits through a gaseous disk. With simple numerical models, we show that super-Earths can interact with the gas through dynamical friction to settle in the remote outer regions of a planetary system. Outcomes depend on planet mass, the initial scattered orbit, and the evolution of the time-dependent disk. Efficient orbital damping by dynamical friction requires planets at least as massive as the Earth. More massive, longer-lived disks damp eccentricities more efficiently than less massive, short-lived ones. Transition disks with an expanding inner cavity can circularize orbits at larger distances than disks that experience a global (homologous) decay in surface density. Thus, orbits of remote planets may reveal the evolutionary history of their primordial gas disks. A remote planet with an orbital distance ~ 100 AU from the Sun is plausible and might explain correlations in the orbital parameters of several distant trans-Neptunian objects.

Subject headings: Planetary systems – Planets and satellites: formation – planet disk interactions

1. Introduction

The formation of gas giants is a fast process limited by the lifetime of the gas in a circumstellar disk. In core accretion models, solids coalesce rapidly into $\sim 10 M_{\oplus}$ planets, which then accrete gas to become full-fledged giants (Pollack et al. 1996). The core formation step is uncertain. A plausible mechanism involves large (1-1000 km) seed objects that form quickly by gravitational streaming

instabilities (Johansen et al. 2007; Dittrich et al. 2013) and then accrete pebbles and collision fragments which interact aerodynamically with the gas (Kenyon & Bromley 2009; Kobayashi et al. 2011; Bromley & Kenyon 2011a; Lambrechts & Johansen 2012; Chambers 2014). Once a few large cores form, competition for the remaining fragments and pebbles favors the most massive proto-planets. As gas giants begin to carve out gaps in the disk, numerical simulations show that gas giants gravitationally scatter other massive cores, leftover planetesimals, and other less massive objects (e.g., Chatterjee et al. 2008; Bromley & Kenyon 2011a).

Scattering appears to play a major role in setting the orbital architecture of many planetary systems. Dynamical interactions between gas giants and leftover large planetesimals stabilized the outer solar system (e.g., Tsiganis et al. 2005; Morbidelli 2013). Among exoplanets, scattering can explain the high orbital eccentricities of ice and gas giants close to the host star (e.g., Jurić & Tremaine 2008; Ford & Rasio 2008; Chatterjee et al. 2008). At the other extreme, free-floating planets can result from ejection during a strong gravitational encounter with a more massive planetary companion (Levison et al. 1998). Weaker encounters result in planets which are scattered outward but remain bound to the host star (e.g., Bromley & Kenyon 2011a, Figs. 14–16).

With initial trajectories resembling the orbits of long-period comets, the ultimate fate of planets on eccentric orbits far from their host stars depends on their interactions with the gas and solids remaining in the protoplanetary disk. In a low mass disk, weak interactions probably prevent the orbit from circularizing, leaving the planet on an eccentric orbit and risking additional interactions with more massive planets closer to the host star. If circularization is possible in a more massive disk, the scattered planet may find a stable orbit far from its birthplace.

Quantifying the probability of scattering and subsequent circularization of giant planets has clear observational implications. Among the known exoplanets, the 1.5 M_{\odot} star HR 8799 has a planetary system with four super-Jupiters on low eccentricity orbits with semimajor axes of roughly 15–70 AU (Marois et al. 2008; Currie et al. 2012b). Although migration from 5–10 AU is a popular model for producing at least some of the observed planets (e.g., Hahn & Malhotra 1999; Crida et al. 2009; Raymond & Bonsor 2014), scattering followed by circularization is a plausible alternative. With a highly eccentric orbit ($e \sim 0.8$) far from its host star ($a \approx 120$ AU), Fomalhaut b is a promising candidate for a low mass planet scattered during a strong gravitational encounter with a more massive planet (Kalas et al. 2008, 2013; Beust et al. 2014; Tamayo 2014). However, the mass of the planet and the orbital eccentricity remain very uncertain (e.g., Currie et al. 2012a; Kenyon et al. 2014). As direct imaging reveals larger samples of exoplanets on wide orbits (Macintosh et al. 2014; Tamura 2014), robust constraints on the physical conditions required for scattering and circularization will enable better evaluations of plausible formation mechanisms for these systems.

Here, we describe outcomes for planets scattered into remote regions of their planetary systems during the epoch of gas giant formation. Our main goal is to highlight physical conditions in a protostellar disk which enable a scattered planet to settle into a low-eccentricity orbit at a large

distance from the planet forming region. In §2 we outline the structure and evolution of a disk, along with a prescription for planet-disk interaction by gas drag and dynamical friction. Then, in §3 we present results from simulations of scattered planets as they interact with an evolving disk. Finally, in §4 we summarize our results and put them in context with observations of exoplanetary systems.

2. Scattered planets and protoplanetary disks: preliminaries

To calculate the long-term evolution of interactions between scattered planets and gas disks, we use the N-body component of *Orchestra*, an ensemble of computer codes for the formation and evolution of planetary systems (Bromley & Kenyon 2006; Kenyon & Bromley 2009; Bromley & Kenyon 2011a). This code, with an adaptive 6th order integrator, has passed a stringent set of dynamical tests and benchmarks (e.g., Duncan et al. 1998). We have used the code to simulate scattering of super-Earths by growing gas giants (Bromley & Kenyon 2011a), migration through planetesimal disks (Bromley & Kenyon 2011b) and Saturn’s rings (Bromley & Kenyon 2013), and formation of Pluto’s small satellites (Kenyon & Bromley 2014).

Here, we modify the code to include dynamical friction and aerodynamic drag from the gas disk using analytical approximations for the acceleration (e.g., Ostriker 1999). We then consider the orbits of individual planets scattered onto distant, highly eccentric orbits by one or more larger planets orbiting at smaller distances from the host star. We do not attempt to model planet-planet scattering in detail. Instead, we describe general conditions which lead to a remote planet on an eccentric orbit, dynamically isolated from the rest of the planetary system except for the extended gas disk (§2.1). We then describe our parameterization of the gas disk and its evolution (§2.2), the acceleration on a scattered planet by the disk (§2.3), and the results of simulations (§3).

2.1. Growing cores and planet-planet scattering

Our scenario for creating a remote planet has a key preliminary step, the formation of multiple planetary cores before the gas disk disperses. Within this time frame, at least one of these cores must reach a critical mass, m_{crit} , sufficient to scatter one or more of the other cores to large orbital distance.

We crudely estimate m_{crit} for a core by considering an idealized encounter with a lighter companion. We assume that the larger planet is on a circular orbit. The smaller planet, through previous interactions with other planets, has negligible orbital speed, as if near apoastron on an eccentric orbit. We also assume that the interaction sends the smaller planet radially outward from the host star. Thus, it experiences a 90° deflection in the reference frame of the larger planet. The critical mass then follows from a Rutherford scattering analysis with the constraint that the smaller core must have a distance of closest approach that remains outside of the physical radius

of the larger one:

$$m_{\text{crit}} \approx 10 \left(\frac{a}{5 \text{ AU}} \right)^{-3/2} \left(\frac{\rho}{2 \text{ g/cm}^3} \right)^{-1/2} \left(\frac{M_\star}{1 M_\odot} \right)^{-3/2} M_\oplus \quad (1)$$

where a is the planet’s orbital distance, ρ is its average mass density ($\rho \approx 2 \text{ g/cm}^3$ corresponds to a core with a mixture of ice and rock; see Papaloizou & Terquem 1999), and M_\star is the mass of the central star. In principle, significant outward scattering can occur even as the larger core is just starting to accrete gas from the protostellar disk (Pollack et al. 1996; D’Angelo et al. 2011; Hori & Ikoma 2011; Piso & Youdin 2014). The formation time for a core of this mass is uncertain, but simulations suggest that gas accreting cores can form well within the lifetime of the gas disk (see, for example Kenyon & Bromley 2009; Bromley & Kenyon 2011a).

Numerical simulations of gas giant formation confirm that (a) multiple cores can form, and (b) they can scatter each other to large distances (Bromley & Kenyon 2011a). In typical models that produce multiple planets, over 80% of the 1–15 M_\oplus cores get scattered beyond $\sim 30 \text{ AU}$. Although the timing is uncertain, scattered planets are probably a common outcome of gas giant planet formation.

After scattering by a more massive core, a remote planet’s orbit continues to evolve as it repeatedly encounters the same massive core every periastron passage. There are several reasons to suspect that repeated encounters following a large scattering event do not greatly alter the remote planet’s orbit. First, the time between periastron passages, i.e., the remote planet’s orbital period, is

$$T_{\text{orbital}} = 1000 \left(\frac{a}{100 \text{ AU}} \right)^{3/2} \left(\frac{M_\star}{M_\odot} \right)^{-1/2} \text{ yr}. \quad (2)$$

This time scale is only somewhat shorter than the time scale for the massive core with mass m to migrate through the disk (Ward 1997; Tanaka et al. 2002; Papaloizou et al. 2007):

$$T_{\text{migrate}} \equiv \frac{a}{\dot{a}} \approx 3 \times 10^4 \left(\frac{m}{10 M_\oplus} \right)^{-3/2} \left(\frac{a}{5 \text{ AU}} \right)^{1/2} \left(\frac{M_\star}{M_\odot} \right)^{3/2} \text{ yr} \quad (3)$$

Thus, between each periastron passage of the remote planet, a $10 M_\oplus$ core at 5 AU moves by roughly 0.2 AU. This distance is slightly larger than the massive core’s Hill radius, which defines its gravitational sphere of influence as it orbits the host star. Thus, unless the two planets have a rare orbital commensurability, the larger planet may drift inward, leaving the orbit of the remote planet free from subsequent interactions.

Other mechanisms, such as gravitational perturbations from other planetary cores or nearby stars (if the young host star is in a cluster), may serve to isolate the remote planet from the massive core that scattered it. Interactions between the remote planet and the gas disk may change the planet’s orbit and further isolate it from the massive core. To estimate the time scale for these interactions, we now consider the properties of the gas disk.

2.2. Disk structure and evolution

Once flung outward, the smaller planet interacts with the gas and solid particles in the outer disk. To assess the effect of the disk on a scattered planet’s orbit, we establish the physical properties of circumstellar disks. At early times, disks are massive and extended. For solar-type stars with typical ages of 1–2 Myr, total disk masses are 0.001–0.1 M_{\odot} (Andrews et al. 2013). Disks evolve on a time scale τ of several million years (Haisch et al. 2001) through viscous dissipation (Lynden-Bell & Pringle 1974; Lin & Papaloizou 1980; Lin & Bodenheimer 1982), photoevaporation by the radiation of the host star (Clarke et al. 2001; Owen et al. 2012), and erosion from stellar winds (Ruden 2004; Lovelace et al. 2008). Together, these interactions lead to a general dispersal of the disk, with a monotonic decrease in surface density over time at rates which may depend on orbital distance from the host star (as in the reviews by Alexander et al. 2013; Youdin & Kenyon 2013).

We assume the gaseous component of the disk has an axisymmetric surface density distribution as a function of orbital distance a and time t :

$$\Sigma(a, t) = \Sigma_0 X e^{-t/\tau} \left(\frac{a}{a_0} \right)^{-p}, \quad (4)$$

where the power-law index $p \sim 1$, $\Sigma_0 \equiv 2000 \text{ g/cm}^2$ is a fiducial surface density at distance $a_0 \equiv 1 \text{ AU}$, and the parameter X scales the initial mass of the disk (cf. Pascucci et al. 2004; Piétu et al. 2007; Andrews et al. 2011; Dent et al. 2013; Birnstiel & Andrews 2014).

The disk has a vertical scale height

$$H(a) = h_0 \left(\frac{a}{a_0} \right)^q, \quad (5)$$

where $h_0/a_0 = 0.01\text{--}0.05$ and the power-law index $q = 9/7$ (Chiang & Goldreich 1997). This scale height is proportional to the sound speed in the gas, $c_s \approx H v_{\text{Kep}}/a$, where v_{Kep} is the circular Keplerian speed at orbital distance a . We assume that H and c_s are independent of time.

The gas density within the disk is approximately Σ/H :

$$\rho_{\text{gas}} = \frac{\Sigma_0 X}{h_0} e^{-t/\tau} \left(\frac{a}{a_0} \right)^{-p-q} \quad (6)$$

$$\approx 4.5 \times 10^{-9} \tilde{X} e^{-t/\tau} \left(\frac{a}{1\text{AU}} \right)^{16/7} \text{ g/cm}^3 \quad (p = 1). \quad (7)$$

where

$$\tilde{X} = X \frac{0.03}{h_0/a_0}. \quad (8)$$

Introducing \tilde{X} allows us to parameterize the gas density, which regulates where and when a scattered planet settles in the outer regions of a planetary system.

The final property is the rotation speed of the gaseous disk. We assume material in roughly circular orbits set by the stellar and disk potentials. Gas pressure reduces the orbital velocity by a factor of $(1 - H^2/a^2)$ (e.g., Youdin & Kenyon 2013).

To model the time evolution of the disk, we consider two prescriptions for the monotonic decline in disk surface density. To describe the global loss of gas from viscous processes, equation (4) includes a term which allows us to set the exponential loss of gas on time scales of $\tau = 1\text{--}10$ Myr (cf. Haisch et al. 2001).

To consider the possibility of the inside-out decay that produces a transitional disk, we establish an inner edge at orbital distance a_{in} that linearly expands with time. Defining a constant expansion rate, κ_{in} , the inner edge evolves as:

$$a_{\text{in}}(t) = a_{\text{in}}(0) + \kappa_{\text{in}} t, \quad (9)$$

until the inner edge reaches the fixed outer edge a_{out} . Once $a_{\text{in}} = a_{\text{out}}$, the disk mass reaches zero; interactions between the planet and the gas cease. Numerical simulations (e.g., Owen et al. 2012) and observations of transition disks (Calvet et al. 2005; Currie et al. 2008; Andrews et al. 2011) suggest opening rates of roughly 10 AU/Myr.

If a gas giant starts the dispersal by carving out a gap in the disk, the inside-out removal of disk material is plausible (see Alexander et al. 2013, and references therein). Here, we always assume that a massive gas giant orbiting at roughly 5 AU is responsible for scattering planets into the outer disk. Although the exponential decay of a disk from viscous evolution and the erosion of the disk inner edge by photoevaporation and stellar wind erosion probably occur simultaneously (cf. Ribas et al. 2014), here we consider these modes as separate cases.

2.3. Planet-disk interactions

Planets interact with the gas aerodynamically and gravitationally. Gas flowing by the planet produces aerodynamic drag. The gravity of planets with $M \gtrsim 1 M_{\oplus}$ can create a density wake in the disk; the dynamical friction associated with this wake tends to circularize the planet’s orbit. For both mechanisms, the amount of drag depends on the mass and radius of the planet and the mean density, the sound speed, and other properties of the disk (Dokuchaev 1964; Ruderman & Spiegel 1971; Weidenschilling 1977; Ohtsuki et al. 1988; Ostriker 1999; Adams et al. 2009; Lee & Stahler 2014).

To estimate the net acceleration from these two processes, we calculate

$$\frac{d\vec{v}_{\text{drag}}}{dt} = - \max(a_{\text{aero}}, a_{\text{dyn}}) \frac{\delta\vec{v}}{|\delta\vec{v}|} \quad (10)$$

where $\delta\vec{v}$ is the velocity of the planet in the rest frame of the surrounding gas, and

$$a_{\text{dyn}} = \frac{2\pi G^2 \rho_{\text{gas}} m_{\bullet} \mu^2 (C_{\text{aero}}^2 + C_{\text{dyn}}^2 \mu^2)^{1/2}}{c_s^2 (1 + \mu^2)^{5/2}} \quad (11)$$

$$a_{\text{aero}} = \frac{\pi C_{\text{aero}} r_{\bullet}^2 \rho_{\text{gas}} |\delta \vec{v}|^2}{2m_{\bullet}} \quad (12)$$

are associated with dynamical friction and aerodynamic drag respectively; m_{\bullet} is the planet mass, r_{\bullet} is its physical radius, $\mu \equiv |\delta \vec{v}|/c_s$ is the Mach number, and the C 's are drag coefficients of order unity. We choose the form of the expression for a_{dyn} to give desired results in the low- and high-Mach number regimes, with an interpolation function to cover transonic speeds in the manner of Lee & Stahler (2014). Numerical simulations (e.g. Ruffert 1996) indicate that this type of parameterization is realistic.

We estimate numerical values for the coefficients C_{aero} and C_{dyn} with simple assumptions. In the aerodynamic case, the planet is much larger than the mean free path in the gas. For subsonic speeds, the frictional acceleration is then proportional to $|\delta \vec{v}|^2$. A spherical shape in this (quadratic) regime corresponds to $C_{\text{aero}} = 0.44$ (e.g. Adachi et al. 1976; Weidenschilling 1977).

For supersonic flow, we estimate the magnitude of the dynamical friction force from integrating over the impact parameter b for gas elements as they flow past the planet. Weak scattering theory gives the contribution from each element to the acceleration as $\delta a \sum (b|\delta \vec{v}|)^{-2}$ (e.g. Dokuchaev 1964; Ruderman & Spiegel 1971; Lin & Papaloizou 1979). We consider only more distant encounters with $b > H/2$; on scales smaller than the disk height, random motions of the gas wash out the effect. Then, assuming that the planet is traveling near the midplane of a disk with slab geometry, we integrate over all gas streamlines flowing by, except for those streamlines that come within a distance $H/2$ of the planet in the disk plane¹. Following this prescription, we estimate $C_{\text{dyn}} = 0.62$.

In addition to the small-scale gravitational wakes, planets orbiting within the disk are accelerated by long-range interactions with the full disk. Assuming that the disk on large scales is largely unperturbed by the planet, the disk potential is axisymmetric, determined by disk parameters a_{in} , a_{out} , h_0 , and Σ . For example, in a geometrically-thin power-law disk, the acceleration at orbital distance a near the midplane is

$$\vec{a}_{\text{disk}} = -2\pi C_{\text{grav}} G \Sigma(r) \frac{\vec{r}}{r}, \quad (13)$$

in the limit $a_{\text{in}} \ll a \ll a_{\text{out}}$, where C_{grav} is a constant of order unity that depends on the power-law index p (Bromley & Kenyon 2011a, Appendix A).

In practice, we calculate the unperturbed disk acceleration using a model with constant disk thickness of h_0 , and an efficient numerical algorithm that can accommodate an arbitrary surface density profile (Bromley & Kenyon 2011a).

¹Integration over δa from gas streamlines that pass as close as the surface of the planet yield a coefficient C_{dyn} with approximate logarithmic dependence on physical radius, as in a Coulomb integral (Binney & Tremaine 1987). Here, we exclude streamlines flowing through a square region of dimensions $H \times H$, centered on the planet, as well as any streamlines that lie above or below the slab with elevation $|z| > H/2$, where $\rho_{\text{gas}} = 0$. In the limit of an extended slab, the result is a constant, independent of H . In excluding the contribution from gas flowing near the planet, we underestimate the strength of dynamical friction.

2.4. Limitations of the model

Our approach to the acceleration includes the major large-scale forces, drag and dynamical friction, between the planet and the disk. However, we neglect the differential torques between the planet and disk which generate type I and type II migration (Ward 1997). Our goal instead is to follow the eccentricity damping prior to orbit circularization. The physics in this case depends on the bulk flow of gas, not on the gradient of the flow from Keplerian shear which is central to migration theory (Lin & Papaloizou 1979; Goldreich & Tremaine 1979). While migration can be important once the orbit circularizes (eq. 3), the direction and pace depend on the thermodynamic state of the disk (Paardekooper 2009). To isolate the important issues involved in eccentricity damping, we consider the thermodynamic state fixed and save detailed calculations for a future study.

We also ignore the possibility of additional accretion onto scattered planets as they interact with gas in the outer regions of the disk. If planets accrete (Pollack et al. 1996; Rafikov 2011), they will interact more strongly with the gas, enhancing the effects considered here. Calculations suggest that growth from gas accretion may be important, even for planets as low as a few Earth masses if they are located beyond 100 AU (Piso & Youdin 2014). Thus the orbital damping times in this work are overestimates.

The scenario we propose here and the approximations introduced above have several additional limitations. One concern is the parameterization of the drag force (eq. [10]), particularly in the transonic and subsonic regimes. Fortunately, by the time a planet reaches subsonic speeds, it is already settled in the disk with a relatively low eccentricity, $e \approx H/a \ll 1$. The supersonic regime has more firm analytical basis (e.g., Ostriker 1999, although see Lee & Stahler 2014) that is consistent with numerical simulations (Ruffert 1996). Furthermore, our implementation is conservative in its neglect of interactions between the planet and gas on scales less than the disk height; at supersonic speeds, we might have included streamlines that crossed inside the planet’s Hill sphere.

We also limit the initial orbits of scattered planets to lie in the disk midplane where planet-disk interactions are strongest. When a planet has a significant orbital inclination $i \gtrsim H/a$, it spends only a fraction of its orbit embedded in gas. The orbital evolution is then similar to a system where a planet with small i orbits within a disk with a lower gas surface density, with details that depend on the planet’s orbital elements. Drawing from experience with dynamics in Saturn’s rings (Bromley & Kenyon 2013), we speculate that when a planet starts out with some inclination, it will settle vertically into the disk plane on a time scale similar to the circularization time.

In our calculations, we assume that the formation time for planets is short compared to the evolutionary time scale of the disk. Thus, fully-formed planets scatter at $t = 0$, when the disk has its initial surface density (eq. [4]). Although core formation can be fast, well within ~ 1 Myr (Kenyon & Bromley 2009; Lambrechts & Johansen 2012; Piso & Youdin 2014), the surface density of the disk probably evolves as planets form (e.g., Bromley & Kenyon 2011a). This aspect of our approach tends to overestimate the disk mass available to circularize the planet and underestimate

the damping time. For the $\tau \approx 2\text{--}4$ Myr disk evolution times adopted here, the impact of this assumption is reasonably small.

3. Simulations of planetary relocation

To assess the effect of the disk on a scattered planet we set up a suite of simulations with a variety of disk parameters and planetary orbits around a $1 M_{\odot}$ star. We use disk models with $\Sigma \sim 1/a$ ($p = 1$), $h_0/a = 0.03$, and a density factor \tilde{X} with values of 0.25, 0.5, and 1 (eqs. [4]–[8]). In all cases illustrated in the Figures, the disk starts with $a_{\text{in}} = 20$ AU and $a_{\text{out}} = 200$ AU. Simulations with $a_{\text{in}} = 5$ AU and $a_{\text{out}} = 350$ AU allow us to assess how outcomes depend on the initial extent of the disk. To quantify the subsequent gas loss from the disk, we choose either the exponential decay mode with $\tau = 2$ and 4 Myr, or an expanding inner cavity with $\kappa_{\text{in}} = 20$ and 40 AU/Myr.

The models have initial disk mass that ranges from $0.06 M_{\odot}$ to $0.25 M_{\odot}$. These values are large compared to those of disks around T Tauri stars (Andrews et al. 2013) but more in line with disks around protostars (Andrews & Williams 2005). This trend with stellar age is consistent with the assumption that planets form rapidly (see the discussion in Najita & Kenyon 2014). Still, the most massive disk is probably somewhat unrealistic in terms of surface density and total mass. However, since the key physical quantity for planet-disk interaction is the local density, the models labeled here according to surface density can represent disks with lower (higher) total mass if they have proportionally lower (higher) scale heights.

In our models, scattered planets have (i) masses of 1, 3, 10 and $30 M_{\oplus}$, (ii) initial periastron distances of 10 AU, and (iii) initial apoastron distances of 100, 200 or 300 AU, corresponding to a of 55, 105 AU and 155 AU, with e of 0.82, 0.9 and 0.94, respectively. For each configuration we ran simulations with a Jupiter mass gas giant ($a = 5$ AU, $e = 0$); it had negligible effect on outcomes. The orbits of all planets considered here are coplanar with the disk. In determining orbital elements we incorporate only the central star’s mass, without treating the gravity of the extended disk or the gas giant. We launch all planets from periastron in the plane of the disk and calculate evolution over a 10 Gyr period with a 6th-order integration code (Bromley & Kenyon 2006, 2011a). With the most massive planets in the most massive disks, we omit the orbital evolution after the planet circularizes ($e < 0.01$), as our code is not designed to follow migration in this regime.

3.1. Orbital evolution during disk depletion

To follow the impact of planet-disk interactions, we track the planetary orbital elements throughout each simulation. Figure 1 illustrates the orbital evolution of planets with masses ranging from $1\text{--}30 M_{\oplus}$ in a massive ($\tilde{X} = 1$) disk that decays exponentially with $\tau = 4$ Myr. The more massive planets experience significant circularization within a few million years; less massive

planets remain on eccentric orbits with $e > 0.5$. This strong dependence on planet mass is a direct result of dynamical friction, which generates an acceleration that scales as m_{\bullet} (eq. [11]). As in type I migration, a more massive planet creates a more massive density wake, which feeds back to affect the planet’s orbit. Aerodynamic drag is not important for any of these planets over the disk lifetime.

The jitter in a , e , and q in Figure 1 is an artifact of our approach to deriving orbital elements. To estimate them, we assume osculating orbits in the Keplerian potential of the star. However, at early times when the disk is massive, the osculating orbital elements are affected by perturbations from the disk potential. Furthermore, when elements are sampled as a planet makes radial excursions through the disk, the values of a , e , and q can vary, even over a single orbital period. The result is a modest amount of jitter. Because our goal is to follow trends in elements, this choice for estimating orbital parameters has no impact on our conclusions.

To test the dependence of orbital evolution on disk structure, we consider the evolution of a planet with $m_{\bullet} = 10 M_{\oplus}$ in a disk with gas density parameter $\tilde{X} = 0.25, 0.5$ and 1 (Figure 2). Here we see the clear impact of gas drag: higher gas density (larger \tilde{X}) causes stronger eccentricity damping. Massive planets in disks with $\tilde{X} = 1$ damp on time scales of 1–2 Myr. In less dense disks with $\tilde{X} = 0.25$, there is little damping after 7–8 Myr.

In our models, the acceleration of the planet from dynamical friction depends on the product of gas density and planet mass. Thus we might be tempted to take advantage of this degeneracy and calculate a single suite of simulations as a function of one parameter, $\gamma = m_{\bullet}\rho_{\text{gas}}$. Then we could estimate the behavior of any planet in a disk with some specified gas disk by looking up that simulation with the corresponding value of γ . However, we caution that the acceleration also has dependence on the sound speed in the transonic regime, which can break the $m_{\bullet}\rho_{\text{gas}}$ degeneracy, especially if the disk surface density and scale height are set as free parameters (see §2.2 for details).

Aside from the masses of the disk and planet, the time evolution of the disk surface density also sets the damping time. Figure 3 compares results for $10 M_{\oplus}$ planets embedded in $\tilde{X} = 0.5$ disks with different modes and time scales for disk depletion. Disk lifetime is clearly important. Short-lived disks ($\tau = 2$ Myr) or disks with a rapidly expanding inner edge ($\kappa_{\text{in}} = 40$ AU/Myr) are less efficient at damping planetary orbits than longer-lived disks. In short-lived disks, the acceleration from dynamical friction and gas drag decline too rapidly relative to longer-lived disks. Thus, the eccentricity evolution in a short-lived disk is limited.

In disks with an expanding inner cavity, there are two competing effects. At small a , the increasingly large inner disk radius limits damping and delays circularization compared to disks with a fixed inner radius. At large a , the relatively static density profile enables additional damping compared to the exponential decay models. Combined, these two features of the evolution conspire to produce circular orbits at larger a than in the exponential decay models.

When the size of the inner cavity expands rapidly, the inner edge of the disk often passes by the planet. This evolution freezes the orbital elements well before the orbit circularizes.

Overall, the details of disk dissipation clearly have a large impact on the fate of scattered planets. In disks decaying exponentially on long time scales, massive planets achieve circular orbits at small a . When disks have slowly growing inner cavities, massive planets achieve circular orbits at much larger a . Even lower mass planets whose periastron distance grows only modestly by virtue of eccentricity damping can have a growing semimajor axis (e.g., upper right panel in Fig. 3). Thus, measuring the orbital elements for large ensembles of planets with $a \approx 20\text{--}100$ AU might provide some insight into the time evolution of the disk surface density.

3.2. Simulation results and the final orbital configurations

Figure 4 illustrates the outcomes of the simulations, showing final orbits for each disk configuration distinguished by surface density (increasing with vertical position of the central stars in the plot) and disk evolution mode (exponential decay on the left and expanding inner cavity disk on the right). A comparison between individual panels illustrates that the outcomes depend on how effectively the gas can act on a planet before the gas vanishes.

In the left two columns, the graphic emphasizes the point that planets tend to circularize relatively close, $a \approx 40$ AU, to the host star. Damping depends on the disk lifetime: planets circularize more easily in long-lived disks than in short-lived disks. Independent of the disk lifetime, massive planets circularize more easily than low mass planets. For the disks in this study, $10\text{--}30 M_{\oplus}$ planets achieve circular orbits; $1\text{--}5 M_{\oplus}$ planets remain on eccentric orbits.

In the right two columns, the diagram illustrates how circularization depends on the mode of disk dispersal. Expanding inner cavities tend to leave planets on orbits with large a . Disks with slowly expanding inner cavities have more time to circularize planetary orbits than disks with rapidly expanding cavities. As with exponentially decaying disks, $10\text{--}30 M_{\oplus}$ planets circularize much more frequently than smaller mass planets.

Overall, disks with expanding inner cavities yield planets with a broader range of a and e than the exponentially decaying disks. In the cavity models, varying the disk mass and the expansion time provide a larger range of circularization time scales compared to the exponentially decaying disks. Thus, exponentially decaying disks circularize a few massive planets and leave the rest on orbits with elements similar to their initial elements. Disks with expanding cavities have time to fill the space between circular and high e orbits.

Figure 5 focuses specifically on eccentricity damping. It shows the final eccentricity for models grouped by planet mass. As in the previous figures, the dependence is clear: planets with larger mass interact more strongly, with strong eccentricity damping for the most massive planets, the Neptune analogs in our runs. The Earth-mass planets experience comparatively little damping. Planets with masses between these two limits have eccentricities that are most sensitive to the details of the disk and its evolution.

Making other choices for a_{in} and a_{out} leads to qualitatively similar results. When $a_{\text{in}} < q = a(1 - e)$, circularization occurs earlier and at smaller orbital distance. This effect is strongest in exponentially decaying disks and for the most massive planets. For example, in an exponentially decaying disk ($\tilde{X} = 0.5$, $\tau = 4$ Myr) with the inner edge moved to $a_{\text{in}} = 5$ AU, a $30 M_{\oplus}$ planet with an initial apoastron distance of 200 AU ($a = 105$ AU, $e = 0.9$) ends up on a circular orbit at $a \approx q \approx 30$ AU, compared to 40 AU in our baseline case with the more distant inner disk edge.

Extending the outer edge of the disk past the initial apoastron distance has the opposite effect. In our baseline simulations one set of scattered planets has an initial apoastron distance of $a(1 + e) = 300$ AU, past the edge of the disk at $a_{\text{out}} = 200$ AU. Extending the disk edge to 350 AU causes orbits to settle at larger final periastron distances; the more massive planets can circularize at greater orbital distances. Because the gas density is lower at larger distances, the effect is significant only if the inner edge is expanding.

Details of disk dispersal also matter. In an extreme case, a $30 M_{\oplus}$ planet achieves a circularized orbit at $a \approx q \approx 150$ AU in a low-mass, extended disk with a slowly expanding inner edge ($\tilde{X} = 0.25$, $a_{\text{out}} = 350$ AU, and $\kappa_{\text{in}} = 20$ AU/yr). For comparison, the same planet in a similar disk with an inner edge at 200 AU circularizes around $a \approx q \approx 100$ AU.

3.3. Summary of simulation results

Our suite of simulations shows a variety of outcomes, with several clear trends.

- Circularization of eccentric orbits is most effective for massive planets, which create the strongest wakes in the gas disk. The orbits of Earth-mass or smaller planets tend to remain eccentric. More massive super-Earths circularize well within the lifetime of a disk, and may initiate Type I radial migration and/or continue to grow by gas accretion.
- Disks with exponential decay in surface density generally damp the orbits of scattered planets, drawing them inward to smaller orbital distances. Only the more massive super-Earths and Neptunes circularize. All low eccentricity orbits reside inside 50 AU. Smaller planets can achieve moderately eccentric orbits at larger orbital distances.
- Disks with an expanding inner cavity have a broader range of outcomes. Super-Earths can circularize beyond 100 AU, depending on when the expanding inner edge of the disk overtakes their orbital distance. Smaller planets can be pushed outward to orbital distances in excess of 200 AU, although their eccentricity remains high.

Additional simulations test other aspects of this model. For example, by adjusting the surface density profile index p (eq. [4]), we find that a steeper (shallower) disk surface density profile tends to circularize planets less (more) efficiently for a given Σ_0 and at smaller (larger) orbital distances.

4. Discussion

We investigate a scenario that allows scattered planets to acquire circular orbits in remote regions of planetary systems through interaction with an extended gas disk. This work is motivated by earlier simulations of gas giant formation (Bromley & Kenyon 2011a), in which super-Earths (failed gas giant cores) are scattered onto stable, eccentric orbits at large semimajor axes. Here, we use a simple parameterization of the acceleration that a planet experiences from dynamical friction and aerodynamical drag, and we calculate orbits around a Sun-like star with an evolving gas disk. Our focus is on eccentricity damping, not on any radial migration from differential torques (Lin & Papaloizou 1979; Goldreich & Tremaine 1979; Ward 1997) that might occur after the planet settles onto a circular orbit.

Our numerical models show that the final orbits of scattered planets depend primarily on their mass. For disks on the high-mass end of the distribution observed in T Tauri disks (e.g., Andrews et al. 2013), planets more massive than the Earth experience substantial orbital evolution. Neptunes damp efficiently. Earth mass planets damp little. Because eccentricity and inclination are generally correlated, the models yield clear correlations between planet mass and the orbital elements e and i .

Precise predictions for orbital architectures accessible with direct imaging depend on how the circumstellar disk vanishes. If mass simply decays exponentially with time everywhere in the disk, our models predict super-Earth and Neptune mass planets on low e orbits close to the host star. However, current data suggest that the transition disks have expanding inner cavities (Ribas et al. 2014). In these disks, we expect massive planets on roughly circular orbits at larger distances from the host star.

These correlations between the planet mass and the final semimajor axis and eccentricity are much different from migration models, where planets remain on circular orbits unless perturbed by another nearby planet (Ward 1997). Models for *in situ* formation also leave massive planets on fairly circular orbits (Helled et al. 2013). Identification of the trends predicted by the simulations would help to distinguish scattering from *in situ* formation and Type I radial migration.

The frequency of remote super-Earths—put in place according to our scenario—depends on the prevalence of massive circumstellar disks. Our models require a relatively massive disk, with $\Sigma_0 \geq 500 \text{ g/cm}^2$ at 1 AU. With a power-law index of $p = 1$, our models have total disk mass in excess of $0.07 M_\odot$. Observations of young stellar systems show a wide range of disk masses and configurations (e.g., Piétu et al. 2007; Andrews et al. 2011; Dent et al. 2013; Piétu et al. 2014). Thus, remote super-Earths may be possible around only $\lesssim 10\%$ of stars (cf. Andrews et al. 2013; Najita & Kenyon 2014). Fortunately, these same massive disks are the most likely to produce multiple super-Earths and the larger planets needed to scatter them (Bromley & Kenyon 2011a). Neptune analogs or more massive scattered planets may be able to settle in even less massive disks. We will explore this possibility in future work.

Imaging observations and planned surveys with Gemini Planet Imager (Macintosh et al. 2014), Subaru (Tamura 2014) and other facilities are beginning to map out the frequency of distant planets around their host stars. The detections are presently limited to Jupiter-size objects beyond roughly 10 AU. Extending these observations to lower mass planets with larger semimajor axes may yield tests of our models.

The planets around HR 8799 (Marois et al. 2008) show the promise of imaging surveys. This planetary system has four super-Jupiters likely on low eccentricity orbits (Currie et al. 2012b), with the most distant at roughly 70 AU from its $1.5 M_{\odot}$ host star. The masses of these planets are much greater than in our models, but if they follow the trend of rapid circularization with increasing mass, then processes described here may have been at work in damping the outer planets to their observed orbital configuration.

Planet-disk interactions may also have contributed to the dynamics of the early solar system. Beyond the orbit of Neptune, icy objects such as Sedna (Brown et al. 2004) are too small to interact with a massive gaseous disk. However, correlations in the orbital parameters of Sedna and similar objects have led to speculation that a super-Earth with mass $2\text{--}15 M_{\oplus}$ resides on a low-eccentricity orbit between 200 AU and 300 AU (Trujillo & Sheppard 2014). If this planet exists, *in situ* formation (Kenyon & Bromley 2004; Stern 2005) and migration from inside 30 AU (Morbidelli 2013) seem unlikely. If the planet is massive and interacted with a massive, extended disk that dispersed from the inside out, formation at small a followed by scattering is plausible. Discovering this planet – barely below the current threshold of detectability (Trujillo & Sheppard 2014) – would provide an excellent test of our scenario and might give us a new probe into the structure and evolution of the Sun’s circumstellar disk.

We are grateful to M. Geller for comments and advice on presentation. We also appreciate the thoughtful comments of an anonymous referee. We acknowledge NASA for a generous allotment of computer time on the NCCS ‘discover’ cluster. Portions of this project were supported by the *NASA Astrophysics Theory* and *Origins of Solar Systems* programs through grant NNX10AF35G, and the *NASA Outer Planets Program* through grant NNX11AM37G.

REFERENCES

- Adachi, I., Hayashi, C., & Nakazawa, K. 1976, *Progress of Theoretical Physics*, 56, 1756
- Adams, F. C., Cai, M. J., & Lizano, S. 2009, *ApJ*, 702, L182
- Alexander, R., Pascucci, I., Andrews, S., Armitage, P., & Cieza, L. 2013, *Protostars and Planets VI* (in press; arXiv:1311.1819)
- Andrews, S. M., Wilner, D. J., Espaillat, C., et al. 2011, *ApJ*, 732, 42

- Andrews, S. M., Wilner, D. J., Hughes, A. M., et al. 2012, *ApJ*, 744, 162
- Andrews, S. M., Rosenfeld, K. A., Kraus, A. L., & Wilner, D. J. 2013, *ApJ*, 771, 129
- Andrews, S. M., & Williams, J. P. 2005, *ApJ*, 631, 1134
- Batygin, K., Brown, M. E., & Betts, H. 2012, *ApJ*, 744, L3
- Beust, H., Augereau, J.-C., Bonsor, A., et al. 2014, *A&A*, 561, A43
- Binney, J., & Tremaine, S. 1987, *Galactic Dynamics* (Princeton: Princeton University Press)
- Birnstiel, T., & Andrews, S. M. 2014, *ApJ*, 780, 153
- Bromley, B., & Kenyon, S. J. 2006, *AJ*, 131, 2737
- Bromley, B. C., & Kenyon, S. J. 2011a, *ApJ*, 731, 101
- Bromley, B. C., & Kenyon, S. J. 2011b, *ApJ*, 735, 29
- Bromley, B. C., & Kenyon, S. J. 2013, *ApJ*, 764, 192
- Brown, M. E., Trujillo, C., & Rabinowitz, D. 2004, *ApJ*, 617, 645
- Calvet, N., D’Alessio, P., Watson, D. M., et al. 2005, *ApJ*, 630, L185
- Chambers, J. E. 2014, *Icarus*, 233, 83
- Chatterjee, S., Ford, E. B., Matsumura, S., & Rasio, F. A. 2008, *ApJ*, 686, 580
- Chiang, E. I., & Goldreich, P. 1997, *ApJ*, 490, 368
- Clarke, C. J., Gendrin, A., & Sotomayor, M. 2001, *MNRAS*, 328, 485
- Crida, A., Masset, F., & Morbidelli, A. 2009, *ApJ*, 705, L148
- Currie, T., Debes, J., Rodigas, T. J., et al. 2012a, *ApJ*, 760, L32
- Currie, T., Fukagawa, M., Thalmann, C., Matsumura, S., & Plavchan, P. 2012b, *ApJ*, 755, L34
- Currie, T., Kenyon, S. J., Balog, Z., et al. 2008, *ApJ*, 672, 558
- D’Angelo, G., Durisen, R. H., & Lissauer, J. J. 2011, *Exoplanets*, edited by S. Seager. Tucson, AZ: University of Arizona Press, 2011, 526 pp. ISBN 978-0-8165-2945-2., p.319-346, 319
- Dent, W. R. F., Thi, W. F., Kamp, I., et al. 2013, *PASP*, 125, 477
- Dittrich, K., Klahr, H., & Johansen, A. 2013, *ApJ*, 763, 117
- Dokuchaev, V. P. 1964, *Soviet Ast.*, 8, 23

- Duncan, M. J., Levison, H. F., & Lee, M. H. 1998, *AJ*, 116, 2067
- Ford, E. B., & Rasio, F. A. 2008, *ApJ*, 686, 621
- Galicher, R., Rameau, J., Bonnefoy, M., et al. 2014, *A&A*, 565, L4
- Goldreich, P., & Tremaine, S. 1979, *ApJ*, 233, 857
- Guilet, J., Baruteau, C., & Papaloizou, J. C. B. 2013, *MNRAS*, 430, 1764
- Hahn, J. M., & Malhotra, R. 1999, *AJ*, 117, 3041
- Haisch, K. E., Jr., Lada, E. A., & Lada, C. J. 2001, *ApJ*, 553, L153
- Helled, R., Bodenheimer, P., Podolak, M., et al. 2013, arXiv:1311.1142
- Hori, Y., & Ikoma, M. 2011, *MNRAS*, 416, 1419
- Hoyle, F., & Lyttleton, R. A. 1941, *MNRAS*, 101, 227
- Johansen, A., Oishi, J. S., Mac Low, M.-M., et al. 2007, *Nature*, 448, 1022
- Jurić, M., & Tremaine, S. 2008, *ApJ*, 686, 603
- Kalas, P., Graham, J. R., Chiang, E., et al. 2008, *Science*, 322, 1345
- Kalas, P., Graham, J. R., Fitzgerald, M. P., & Clampin, M. 2013, *ApJ*, 775, 56
- Keane, J. T., Pascucci, I., Espaillat, C., et al. 2014, arXiv:1404.0709
- Kennedy, G. M., & Kenyon, S. J. 2008, *ApJ*, 673, 502
- Kenyon, S. J., & Bromley, B. C. 2001, *AJ*, 121, 538
- Kenyon, S. J., & Bromley, B. C. 2002a, *AJ*, 123, 1757
- Kenyon, S. J., & Bromley, B. C. 2004, *AJ*, 127, 513
- Kenyon, S. J., & Bromley, B. C. 2006, *AJ*, 131, 1837
- Kenyon, S. J., & Bromley, B. C. 2009, *ApJ*, 690, L140
- Kenyon, S. J., & Bromley, B. C. 2010, *ApJS*, 188, 242
- Kenyon, S. J., & Bromley, B. C. 2014, *AJ*, 147, 8
- Kenyon, S. J., Currie, T., & Bromley, B. C. 2014, *ApJ*, 786, 70
- Kenyon, S. J., & Luu, J. X. 1998, *AJ*, 115, 2136
- Kobayashi, H., Tanaka, H., & Krivov, A. V. 2011, *ApJ*, 738, 35

- Lambrechts, M., & Johansen, A. 2012, *A&A*, 544, A32
- Lee, A. T., & Stahler, S. W. 2014, *A&A*, 561, A84
- Levison, H. F., Lissauer, J. J., & Duncan, M. J. 1998, *AJ*, 116, 1998
- Lin, D. N. C., & Bodenheimer, P. 1982, *ApJ*, 262, 768
- Lin, D. N. C., & Papaloizou, J. 1979, *MNRAS*, 186, 799
- Lin, D. N. C., & Papaloizou, J. 1980, *MNRAS*, 191, 37
- Lovelace, R. V. E., Romanova, M. M., & Barnard, A. W. 2008, *MNRAS*, 389, 1233
- Lynden-Bell, D., & Pringle, J. E. 1974, *MNRAS*, 168, 603
- Macintosh, B., Graham, J. R., Ingraham, P., et al. 2014, arXiv:1403.7520
- Marois, C., Macintosh, B., Barman, T., et al. 2008, *Science*, 322, 1348
- Morbidelli, A. 2013, *Planets, Stars and Stellar Systems. Volume 3: Solar and Stellar Planetary Systems*, 63
- Najita, J. R., & Kenyon, S. J. 2014, *MNRAS*, submitted
- Ohtsuki, K., Nakagawa, Y., & Nakazawa, K. 1988, *Icarus*, 75, 552
- Ostriker, E. C. 1999, *ApJ*, 513, 252
- Owen, J. E., Clarke, C. J., & Ercolano, B. 2012, *MNRAS*, 422, 1880
- Papaloizou, J. C. B., Nelson, R. P., Kley, W., Masset, F. S., & Artymowicz, P. 2007, *Protostars and Planets V*, 655
- Papaloizou, J. C. B., & Terquem, C. 1999, *ApJ*, 521, 823
- Paardekooper, S.-J. 2009, *A&A*, 506, L9
- Pascucci, I., Wolf, S., Steinacker, J., et al. 2004, *A&A*, 417, 793
- Piétu, V., Dutrey, A., & Guilloteau, S. 2007, *A&A*, 467, 163
- Piétu, V., Guilloteau, S., Di Folco, E., Dutrey, A., & Boehler, Y. 2014, *A&A*, 564, A95
- Piso, A.-M. A., & Youdin, A. N. 2014, *ApJ*, 786, 21
- Pollack, J. B., Hubickyj, O., Bodenheimer, P., Lissauer, J. J., Podolak, M., & Greenzweig, Y. 1996, *Icarus*, 124, 62
- Rafikov, R. R. 2011, *ApJ*, 727, 86

- Rasio, F. A., & Ford, E. B. 1996, *Science*, 274, 954
- Raymond, S. N., & Bonsor, A. 2014, *MNRAS*, 442, L18
- Ribas, Á., Merín, B., Bouy, H., & Maud, L. T. 2014, *A&A*, 561, A54
- Ruden, S. P. 2004, *ApJ*, 605, 880
- Ruderman, M. A., & Spiegel, E. A. 1971, *ApJ*, 165, 1
- Ruffert, M. 1996, *A&A*, 311, 817
- Shima, E., Matsuda, T., Takeda, H., & Sawada, K. 1985, *MNRAS*, 217, 367
- Stern, S. A. 2005, *AJ*, 129, 526
- Tamayo, D. 2014, *MNRAS*, 438, 3577
- Tamura, M. 2014, *IAU Symposium*, 299, 12
- Tanaka, H., Takeuchi, T., & Ward, W. R. 2002, *ApJ*, 565, 1257
- Trujillo, C. A., & Sheppard, S. S. 2014, *Nature*, 507, 471
- Tsiganis, K., Gomes, R., Morbidelli, A., & Levison, H. F. 2005, *Nature*, 435, 459
- Ward, W. R. 1997, *Icarus*, 126, 261
- Weidenschilling, S. J. 1977, *MNRAS*, 180, 57
- Youdin, A. N., & Kenyon, S. J. 2013, *Planets, Stars and Stellar Systems. Volume 3: Solar and Stellar Planetary Systems*, 1

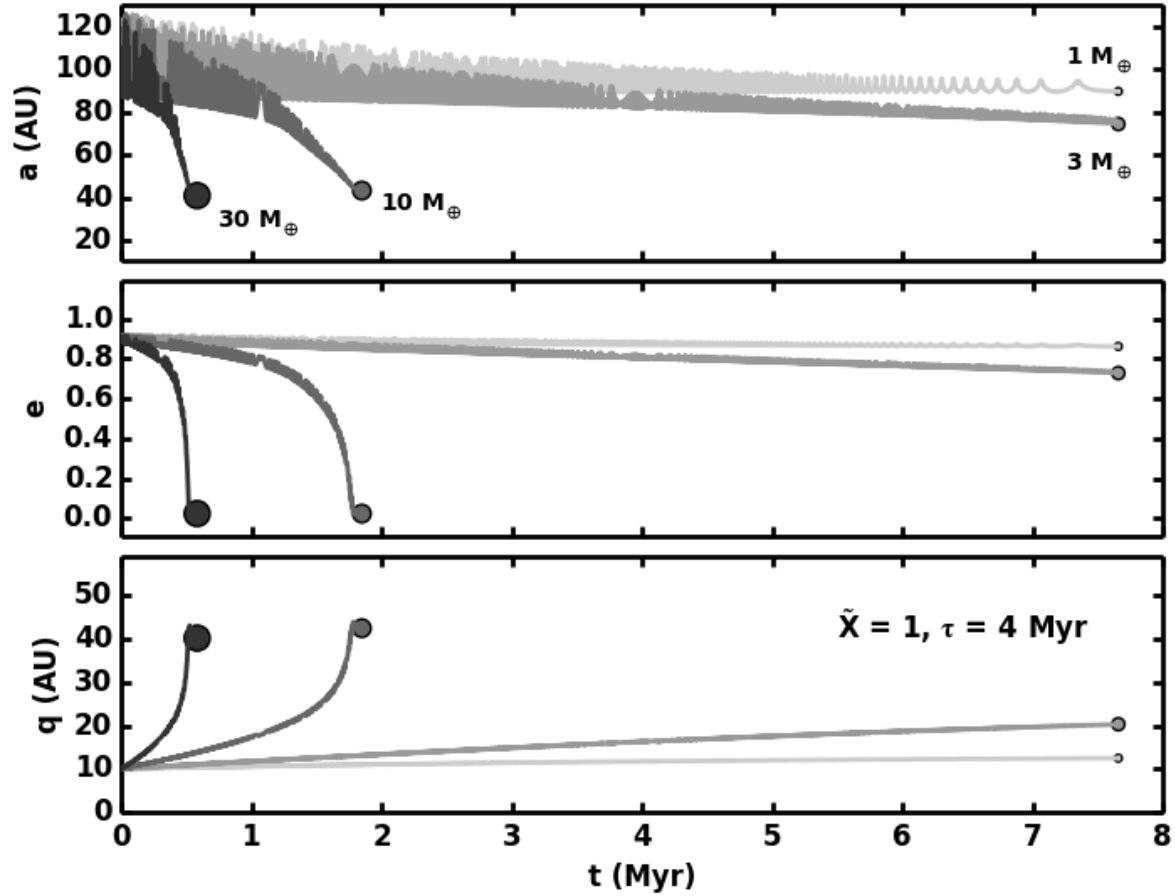


Fig. 1.— Evolution of planetary orbits in an exponentially decaying disk as a function of planet mass. Each track follows the evolution of a planet after it was placed on an orbit with an apoastron distance of 200 AU, in a disk with density parameter $\tilde{X} = 1$ and decay time scale of $\tau = 4$ Myr. Planet masses are labeled in the upper panel. In all panels, the darker shade tracks correspond to the more massive planets. The trend illustrates the correlation of eccentricity damping with planet mass as a result of dynamical friction: a more massive planet can create a bigger density wake, which in turn has a stronger effect on its orbit. The high variability in the orbital elements, particularly the semimajor axis (upper panel), is an artifact of our estimators, which measure osculating parameters as if the disk were massless.

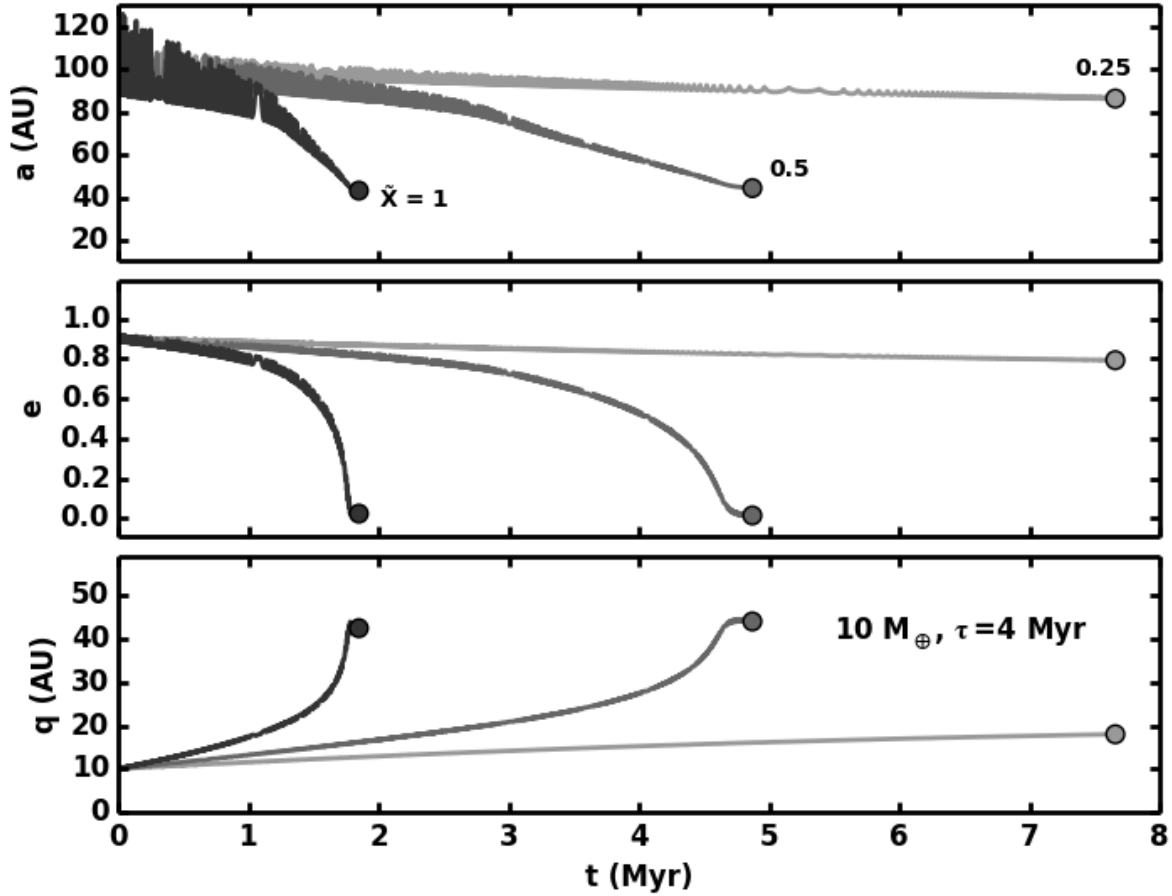


Fig. 2.— Evolution of orbits in disks with different density parameters. Orbits start off as in the previous figure, but in this case a $10 M_{\oplus}$ planet lies in disks with $\tilde{X} = 0.25, 0.5,$ and $1,$ as labeled in the upper panel. Darker shade of the lines and symbols indicates disks with higher density. The effect of the gas density is clear: higher ρ_{gas} means a planet can create a more significant gravitational wake, hence it experiences stronger eccentricity damping.

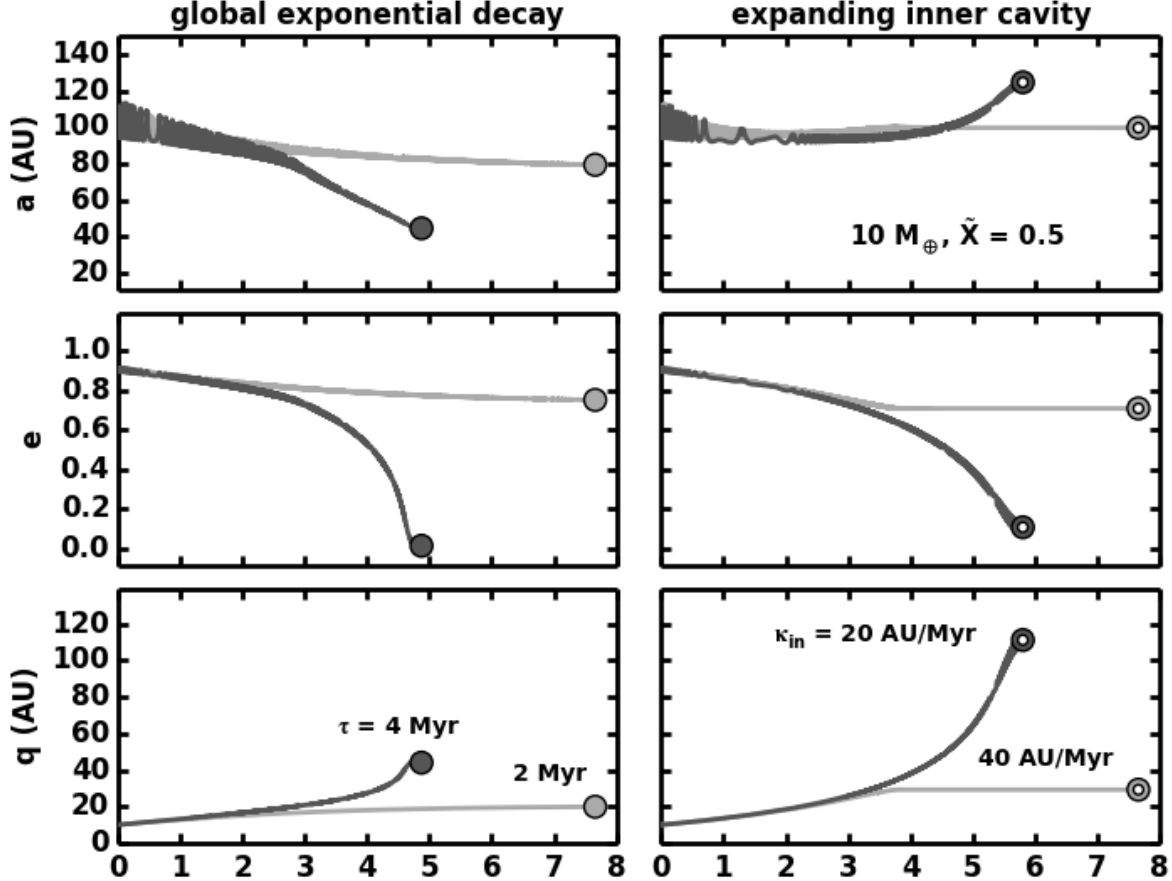


Fig. 3.— Evolution of orbits in disks with varying gas dispersal modes and time scales. Orbits are shown for a $10 M_{\oplus}$ planet in disks with $\tilde{X} = 0.5$. Disks evolve either by an exponential decay in density (left panels) or with an expanding inner cavity (right panels). The time scales for dispersal are 2 and 4 Myr in the cases of exponential decay. The growth rate is 20 and 40 AU/Myr for disks with an expanding inner cavity. The darker shaded curves designate a longer-lived disk. A comparison within each panel shows that longer-lived disks cause more orbital evolution; a comparison between left and right panels illustrates that damping is more effective with a globally decaying disk, but that planets settle at larger orbital distances from their host star in the case of an expanding inner cavity. The planet in a disk with a rapidly growing cavity (light shaded curve and doughnut shaped symbols) experienced orbital evolution until the inner edge of the disk expanded beyond it, at about 4 Myr. With the more slowly expanding inner edge, the planet was able to circularize.

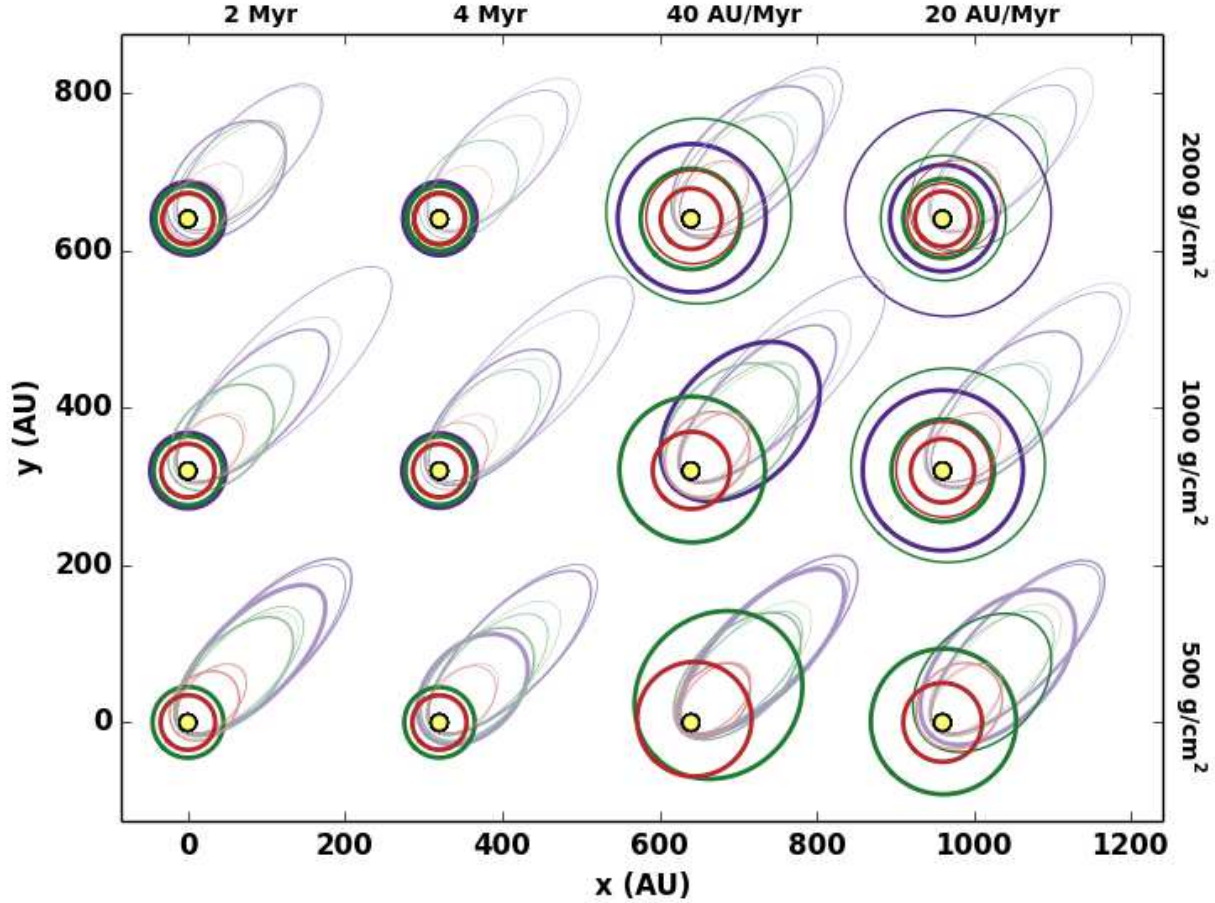


Fig. 4.— Simulation outcomes depicted as elliptical orbital paths for a suite of models. The x - y coordinates give planetary positions in their orbital plane; models are offset from one another so that they are sorted in rows and columns according to model parameters. The first and second columns correspond to exponentially decaying disks with $\tau = 2$ and 4 Myr, respectively. The third and fourth columns have disks with expanding inner edges with rates of $\kappa_{\text{in}} = 40$ and 20 AU/Myr, with the more slowly expanding gap on the far right. In each diagram the line weight corresponds to planet mass (1, 3, 10, and 30 M_{\oplus}), while the color indicates the initial apoastron distance (100 AU is red, 200 AU is green and 300 AU is blue). Only the heavily shaded trajectories have settled to periastron distances beyond Neptune’s orbit.

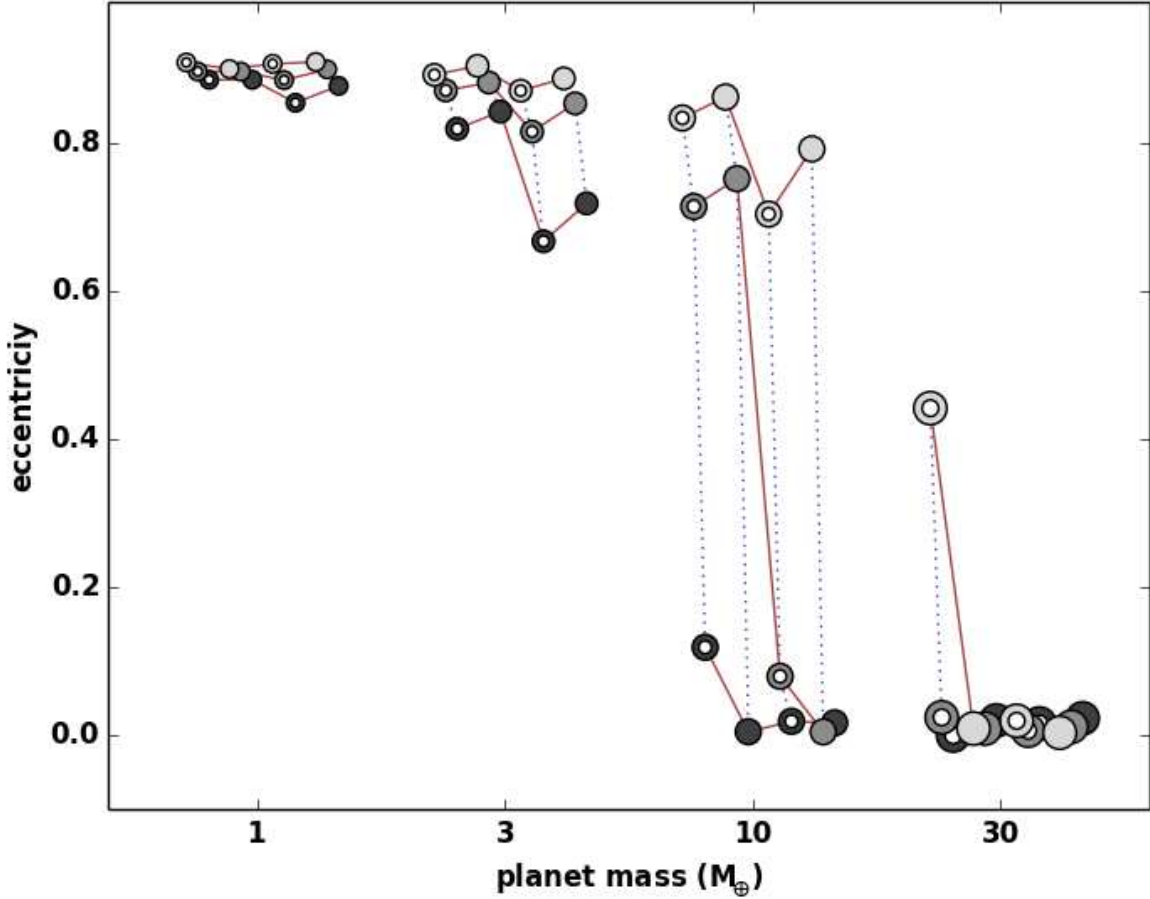


Fig. 5.— The final eccentricity of planets with various masses, reflecting dependence on disk mass and the mode of disk depletion—exponential decay or an expanding inner cavity. The points are grouped along the horizontal direction by planet mass (1, 3, 10 and 30 M_{\oplus} ; symbol size increases with mass), with slight horizontal offsets to distinguish disk mass and depletion mode. The filled circles have disks that decay exponentially in time ($\tau = 2$ and 4 Myr), while the doughnut-shape symbols represent disk models with an expanding inner cavity ($\kappa_{\text{in}} = 20$ and 40 AU/Myr); Models toward the left have faster depletion times. In all cases, the planets are initially on orbits with a semimajor axis of 100 AU and an eccentricity of 0.8; the model with a small planet, low disk mass and a rapidly expanding cavity (upper left-most symbol) experiences little orbital evolution. As planet mass increases, the eccentricity damping is more effective; all of the 30 M_{\oplus} Neptune analogs (right-most group of symbols) circularize.